Visible light responsive heterostructured α-Bi$_2$O$_3$/ZnO doped β-Bi$_2$O$_3$ photocatalyst for remediation of organic pollutants

Gurpreet Kaur[a], Seema Sharma[b,*], Priti Bansal[c,*]

[a]*Research Scholar of I.K. Gujral Punjab Technical University, Jalandhar-Kapurthala Highway, Kapurthala 144603, India, Tel. +91 91158 45087, email: gurpreet.kaur5087@gmail.com (G. Kaur)*
[b]*Department of Chemistry, Maharaja Ranjit Singh Punjab Technical University, Bathinda 151001, India, Tel. +91 94171 14169, email: paperpubseema@gmail.com (S. Sharma)*
[c]*Department of Applied Sciences, YCoE, Punjabi University Guru Kashi Campus, Talwandi Sabo 151302, Bathinda, India, Tel. +91 94175 40285; Fax +91 1655 220253; email: preet2aanand@yahoo.co.in (P. Bansal)*

ABSTRACT

Novel visible-light active α-Bi$_2$O$_3$/ZnO doped β-Bi$_2$O$_3$ (ZB) photocatalyst was synthesized at different temperatures 400°C (ZB4), 500°C (ZB5), and 600°C (ZB6) by modified sol–gel method. The structural, morphological, compositional, and optical properties of synthesized photocatalyst were characterized using X-ray powder diffraction, field emission scanning electron microscopy, energy dispersive X-rays spectroscopy, Fourier transform infrared spectroscopy, and UV-vis spectroscopy. With an increase in calcination temperature, the bandgap of the prepared photocatalyst increases, and metastable β-phase Bi$_2$O$_3$ changes to α-phase. The photocatalytic activity was evaluated using Alizarin Red S (ARS) as a model organic compound. The rate of degradation was estimated from residual concentration spectrophotometrically. The results revealed that with an increase in calcination temperature, the photocatalytic activity of synthesized ZB photocatalyst decreases. Maximum decolorization efficiency (88%) was shown by the photocatalyst prepared at 400°C which is 29% and 37% higher than that of photocatalyst prepared at 500°C and 600°C, respectively.

Keywords: ZnO; Bi$_2$O$_3$; Photocatalyst; Alizarin Red S; Visible light

1. Introduction

Inorganic semiconductor-based photocatalysis has emerged as a "green" technology for the photocatalytic degradation of recalcitrant organic water pollutants [1,2]. Many semiconductor metal oxides such as TiO$_2$, ZnO, Bi$_2$O$_3$, WO$_3$, Nb$_2$O$_5$, CuO, MgO, Fe$_2$O$_3$, SnO$_2$, UV/Fe$_2$O$_3$, Fe$_2$O$_3$/sunlight [3–7], and metal sulfides such as ZnS, CdS, Bi$_2$S$_3$ [8–10] have been employed as photocatalyst for pollutants degradation. Among them, TiO$_2$ and ZnO have been extensively used as photocatalysts due to their excellent optical and electronic properties [11–13]. But, TiO$_2$ and ZnO can be stimulated by ultraviolet (UV) light due to their wide bandgap (3.37 eV) and this factor greatly limits their photocatalytic application under visible light irradiations [14–16]. Bi$_2$O$_3$ is another widely used photocatalyst, exists in six crystallographic polymorphic forms symbolized as α-, β-, γ-, δ-, ε-, and ω and has bandgap ranging from 2.0 to 3.96 eV depending upon the crystalline phase formed [17–21]. But Bi$_2$O$_3$ shows poor photocatalytic activity due to hasty recombination of the photoinduced electron-hole pairs [22,23].

---

* Corresponding authors.

The photocatalytic activity of Bi_2O_3 is improved by doping with metal ions. Doping of semiconductor oxides helps to increase the lifetime of photogenerated electrons and holes which acts as trapping centers close to the conduction band [24]. Bi_2O_3 doped with transition metal (Pb^{+2}, V^{+5}, Ag^{+1}, and Co^{+2}) showed higher photocatalytic activity than bare Bi_2O_3 under visible light [25]. The metastable β-Bi_2O_3 has been proved to be the best photocatalytic crystalline form due to its lower bandgap energy (~2.5 eV) [26]. Photocatalytic activity of β-Bi_2O_3 can be further enhanced by introducing metal atoms such as Ag, Fe, Au, Pb, and C [27]. The best results for metal doping can be obtained when the radius of doping metal is close to that of other metal, to enable its incorporation into lattice sites [28]. A few studies have been reported related to the doping of Bi_2O_3 semiconductor with ZnO. Chen et al. [29] have examined the photocatalytic activity of ZnO doped Bi_2O_3 prepared by spray pyrolysis method for the treatment of methyl orange. Hou et al. [30] investigated the photocatalytic decomposition of methylene blue using $Bi_{38}ZnO_{58}$ synthesized by a solid-state reaction method.

Besides doping, more attention has been given to the design and synthesis of heterostructured catalysts. To date, large numbers of efficient heterostructures have been developed and used for photocatalytic degradation of various organic pollutants because of the advantage over their corresponding single components. For example, AgI/WO_3/ZnO [31], g-C_3N_4@Fe_3O_4 [32], and rGO/TiO_2 [33] photocatalysts have been prepared for the degradation of different organic pollutants. $MoSe_2$/Ag_3PO_4 heterojunction exhibits enhanced photocatalytic activity because of high oxygen evolution [34]. So far, a variety of Z-scheme photocatalysts have been constructed and explored for energy and environmental applications. For example, Bi_2S_3/$BiVO_4$/$MgIn_2S_4$ [35], Ag/g-C_3N_4(CN)/Bi_3TaO_7(BTO) [36], and MoS_2QD/g-C_3N_4 [37] showed excellent photocatalytic activity for the degradation of carbamazepine, sulfamethoxazole, and rhodamine B, respectively. g-C_3N_4/Ag_2MoO_4/Ag_3PO_4 composite photocatalyst exhibits superior solar-driven oxygen evolution [38].

To the best of our knowledge, the synthesis, characterization and application of heterostructure α- and β-form of Bi_2O_3 doped with ZnO photocatalyst has not been reported. In the present work, heterostructured α-Bi_2O_3/ZnO doped β-Bi_2O_3 has been prepared and characterized. Its photocatalytic activity has been evaluated using ARS as a model pollutant.

2. Experimental

2.1. Catalyst preparation

The photocatalyst was prepared by modified sol–gel method with a molar ratio of Bi:Zn fixed at 1:0.25, using bismuth nitrate pentahydrate ($Bi(NO_3)_3$·$5H_2O$), zinc nitrate hexahydrate ($Zn(NO_3)_3$·$6H_2O$), dextrose ($C_6H_{12}O_6$), ammonia solution (25% with specific gravity 0.91), and nitric acid (98 wt.%) (AR grade, Loba Chemie Pvt., Ltd.). Bismuth nitrate pentahydrate was dissolved in 100 mL of HNO_3 solution (60% v/v, HNO_3) to avoid hydroxylation of Bi^{+3} ions. Further 80 mL of ammonia solution was added under constant stirring, the white precipitate formed was washed with double distilled water several times and was refluxed at 80°C for 4 h in 200 mL solution prepared by adding 100 mL of 0.25 M dextrose solution and 100 mL of 0.25 M zinc nitrate solution. After refluxing, the solution was evaporated on a water bath until the formation of shiny chocolate colored gel. The resulting gel was calcined at different temperatures (400°C, 500°C, and 600°C) for 1 h to obtain a yellow colored powder.

2.2. Characterization

X-ray diffraction (XRD) pattern of the prepared photocatalyst was recorded in the 2θ scan range of 20°–80° using APEX-II CCD diffractometer, Bruker, United States (Cu Kα radiations) operated at 40 kV and 30 mA. The morphology of the samples was examined with field emission scanning electron microscopy (FE-SEM, Carl Zeiss SMARTSEM® V05.06, Carl Zeiss, Germany) with energy dispersive spectra (EDS, XFlash® 6|100, Bruker, United States). The chemical structure and composition of the prepared samples were analyzed by Fourier transform infrared (FTIR) spectroscopy using Spectrum 2, Perkin-Elmer, United States spectrometer. The UV-vis absorbance spectra were obtained using UV-1650$_{PC}$ spectrophotometer, Shimadzu, Japan in the range of 200–800 nm.

2.3. Photocatalytic studies

Photochemical degradation experiments were carried in 500 mL vessel equipped with water circulation system placed in a specially designed four-chambered photoreactor, each chamber equipped with 23 W LED bulbs (2,300 lm) with emission in the wavelength range between 480 and 600 nm. During the irradiation, magnetic stirrers and aquarium aerators were used for homogeneous mixing and aeration of the reaction mixture, respectively. The irradiance remains constant throughout the experiment and was found to be 90 μmol/m²/s. The absorption spectra of the dye solution were recorded using a UV-vis spectrophotometer. For the photocatalytic activity measurements, 0.1 g of photocatalyst (ZB4, ZB5, and ZB6) was added into 100 mL of ARS dye solution (20 mg/L at pH = neutral (6.7)). Before the illumination under visible light, the solution was stirred in dark for 20 min to obtain good dispersion and establish adsorption/desorption equilibrium between the photocatalyst and ARS dye. The solution under constant stirring and aeration was illuminated for 13 h under visible light irradiation. During the experiment, at certain time intervals, samples were withdrawn with the help of a syringe and filtered through a 0.45 μm Whatman syringe filter to record absorption spectra of degraded dye solution using UV-vis spectrophotometer. The degradation efficiency (%) was calculated by using the following equation:

$$\text{Degradation efficiency } (\%) = \left(1 - \frac{A}{A_0}\right) \times 100 \quad (1)$$

where A_0 is the initial absorbance of ARS dye and A is the variable absorbance of ARS dye after different intervals of photo-irradiation [39,40].

3. Results and discussion

3.1. XRD analysis

The crystallinity, crystal phases of synthesized nano photocatalyst, and the effect of calcination were examined by XRD as shown in Fig. 1. From XRD pattern and corresponding 2θ values of diffraction peaks, it can be confirmed that heterojunction of α-Bi$_2$O$_3$ (JCPDS card number 71-2274) and ZnO doped β-Bi$_2$O$_3$ (JCPDS card number 43-0449) is formed at temperature 400°C. Zn^{+2} (0.74 Å) can substitute Bi^{+3} ionic sites (1.17 Å) because of its smaller ionic radius [29]. However, with an increase in calcination temperature the metastable β-Bi$_2$O$_3$ changes slowly to α-Bi$_2$O$_3$ which is confirmed as the intensity of peak at 27.4 increases in ZB6 sample in comparison to ZB4 and ZB5. Moreover, peak at 37.6° (1 1 2) appears in ZB5 corresponding to α-Bi$_2$O$_3$ and its intensity increases in ZB6. Two more peaks at 35° (2 1 0) and 62.9° (0 5 2) corresponding to α-Bi$_2$O$_3$ appear in ZB6. The crystallite size was estimated by applying the Scherrer equation ($D = K\lambda/\beta \cos\theta$) to the full width at half-maximum (FWHM) of the (2 0 1) peak, where β is the half-height width of the diffraction peak, $K = 0.89$ is a coefficient, θ is the diffraction angle (27.96°), and λ is the X-ray wavelength corresponding to the Cu Kα radiations (λ = 1.5406 Å) [40,41]. The mean size of nanoparticles calculated by the Debye–Scherrer formula was found to be ~ 40–50 nm.

3.2. FESEM and EDX analysis

The surface morphology of prepared photocatalyst was analyzed by FESEM (Fig. 2). The FESEM images of prepared photocatalyst show the formation of irregularly shaped clusters of nanoparticles. With the increase in temperature, agglomeration increases. At 600°C, there is the appearance of a flowery arrangement constituted with a bean-shaped cluster decorated densely by nano-grain sized particles. The EDS spectrum of prepared photocatalyst showed Bi, Zn, O peaks indicating that the prepared sample was composed of Bi, Zn, and O elements (Fig. 2). Furthermore, no peak related to any impurity was detected in the EDS spectrum which confirms that the synthesized photocatalyst is pure.
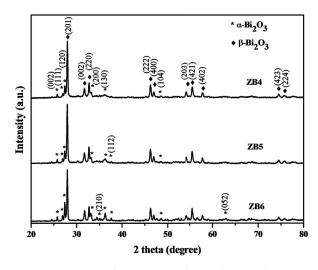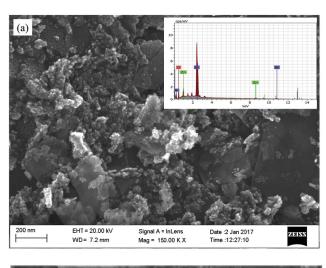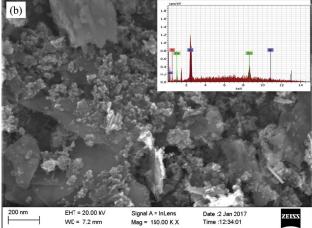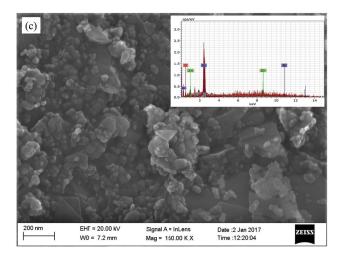

Fig. 2. FESEM images and EDS spectra of (a) ZB4, (b) ZB5, and (c) ZB6 photocatalyst.

3.3. FTIR analysis

The chemical composition of the prepared photocatalyst was examined by Fourier transform infrared (FTIR) spectroscopy (Fig. 3). The peak around 685 cm^{-1} is assigned to the Bi–O stretching vibration of the non-bridging oxygen of the

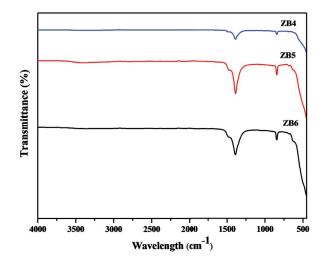Fig. 1. XRD patterns of ZB4, ZB5, and ZB6 photocatalyst.

Fig. 3. FT-IR spectra of ZB4, ZB5, and ZB6 photocatalyst.

distorted Bi–O polyhedra. The peak at 845 cm^{-1} is due to the stretching vibration of Bi–O bonds in BiO$_6$ octahedra. The intense band at 1,389 cm^{-1} possibly arises due to the stretching vibration of the NO$_3^-$ ion [4,22,42,43].
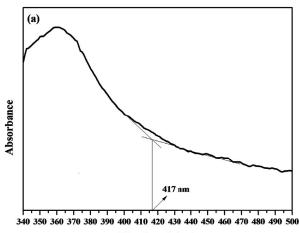
3.4. UV-visible analysis

The optical properties of the synthesized photocatalyst were examined by UV-vis spectrum (Fig. 4) which depicts a strong absorption peak at 417, 409, and 403 nm (defined by the edge at the intersection of wavelength through extrapolation of the horizontal and sharply rising portions of the curves) for ZB4, ZB5, and ZB6, respectively [30]. The bandgap energy of the photocatalyst was calculated using the following equation:

$$\text{Bandgap (eV)} = 1{,}240/\text{Wavelength (nm)} \quad [4,44] \qquad (2)$$
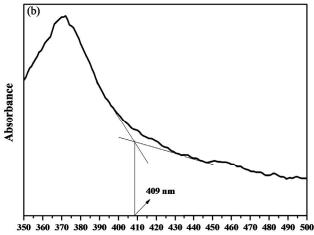
The bandgap of ZB4, ZB5, and ZB6 sample is found to be 2.97, 3.03, and 3.07 eV from the absorption edge. The decrease in absorbance with an increase in calcination temperature is due to the change of β-form (bandgap 2.5 eV) to α-form (bandgap 2.9 eV) of Bi$_2$O$_3$. Moreover, the bandgap of the prepared photocatalyst is more than the pure form of Bi$_2$O$_3$ which confirms its doping with ZnO having bandgap 3.37 eV.

3.5. Photocatalytic activity of the prepared photocatalyst

The photocatalytic activity of prepared photocatalyst was evaluated by photo-degradation of widely used textile dye, Alizarin Red S (sodium alizarin sulfonate, C$_{14}$H$_6$Na$_2$O$_7$S) under visible light irradiation. It is a water-soluble anthraquinone dye and its release in the environment poses a threat to human beings and animal life [45–48]. The activities of the different (ZB4, ZB5, and ZB6) photocatalysts were evaluated by monitoring the UV-vis spectrum of irradiated ARS dye solution. Fig. 5 shows a time-dependent UV-vis spectrum of ARS dye during visible light photoirradiation with a significant decrease in absorption intensity with an
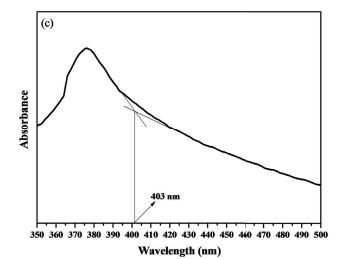

Fig. 4. UV-vis spectra of (a) ZB4, (b) ZB5, and (c) ZB6 photocatalyst.

increase in irradiation time. The spectra of ARS dye shows a peak at 516 nm in the visible region and two narrow peaks at 334 and 261 nm in the UV region. The rate of ARS decolorization was monitored for a decrease in the intensity of
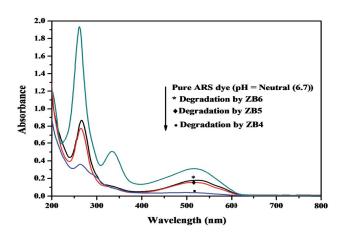
Fig. 5. UV-vis absorption spectral changes of ARS dye solution in the presence of ZB4, ZB5, and ZB6 photocatalyst at neutral pH (6.7) (dye concentration – 20 mg/L, catalyst dose – 0.1 g/100 mL, time – 13 h).
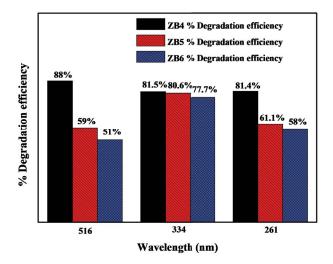

Fig. 6. Comparison of percentage degradation of ARS dye solution (dye concentration – 20 mg/L, pH – 6.7 (neutral), time – 13 h) using ZB4, ZB5, and ZB6 photocatalyst (0.1 g/100 mL) at different peaks 516, 334, and 261 nm.

prominent peak at λ_{max} = 516 nm indicating the degradation of chromatophoric groups of ARS dye [49,50]. The decolorization efficiency was maximum with ZB4 (88%) and only 59% and 51% decolorization was observed with ZB5 and ZB6 within 13 h, respectively. The degradation efficiency of the ARS dye was observed for the decrease in intensity of two narrow peaks at 334 and 261 nm (related to unsaturated bonds). It can also be seen that maximum degradation efficiency was found with ZB4 as compared to ZB5 and ZB6 as shown in Fig. 6.

3.6. Photocatalytic degradation mechanism

Fig. 7 shows the schematic illustration of the photocatalytic mechanism of ZB4 photocatalyst. The feasibility of a photocatalytic activity depends mainly on positions of the valence band maximum and conduction band minimum. The valence band (VB) and conduction band (CB) potentials can be calculated by using the following equation:

$$E_{CB} = X - E^e - 0.5\,E_g \tag{3}$$

where X is the absolute electronegativity of the semiconductor, (X value for Bi_2O_3 is 5.986 eV and for ZnO is 5.79 eV), E^e is the energy of free electrons on the hydrogen scale (~4.5 eV), E_g is the bandgap energy of semiconductor and E_{CB} can be determined by $E_{CB} = E_{VB} - E_g$ [26,51–53]. The conduction band (CB) and valence band (VB) potentials of ZnO, ZB4, ZB5, and ZB6 are given in Table 1.

On irradiation with light conduction band electrons (e^-) and valence band holes (h^+) are generated in the photocatalyst. The conduction band (CB) of doped material is higher in position than ZB4 which can trap electrons (e^-) from conduction band (CB) of semiconductor for the photoreduction of O_2 to produce superoxide radical anion ($O_2^{\bullet-}$) and on protonation further yields HOO$^\bullet$. However, the formed photogenerated holes (h^+) reacts with OH$^-$ or H_2O and oxidize them into OH$^\bullet$ radicals. The resulting OH$^\bullet$ radicals, being
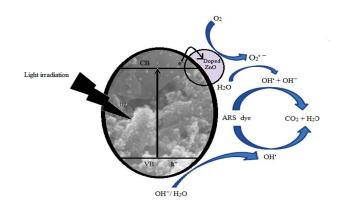

Fig. 7. Schematic diagram of the photocatalytic degradation mechanism of ZB4 photocatalyst.

highly active and strongly oxidizing species are responsible for the oxidation of ARS dye into simple end-products (such as CO_2, O_2, etc.). These reactions can be summarized in the following steps [27,46,54,55]:

$$ZnO/Bi_2O_3 + h\nu \rightarrow e^-\,(CB) + h^+\,(VB) \tag{4}$$

$$OH^- + h^+\,(VB) \rightarrow OH^\bullet \tag{5}$$

$$H_2O + h^+\,(VB) \rightarrow OH^\bullet + H^+ \tag{6}$$

$$O_2 + e^-\,(CB) \rightarrow O_2^{\bullet-} \tag{7}$$

$$O_2^{\bullet-} + H^+ \rightarrow HO_2^\bullet \tag{8}$$

$$HO_2^\bullet + HO_2^\bullet \rightarrow H_2O_2 + O \tag{9}$$

$$H_2O_2 + O_2^{\bullet-} \rightarrow OH^\bullet + OH^- + O_2 \tag{10}$$

Table 1
Bandgap, conduction band (CB), and valence band (VB) values of ZnO, ZB4, ZB5, and ZB6 photocatalysts

Photocatalysts	Bandgap (Eg) (eV)	Conduction band (CB) potential (eV)	Valence band (VB) potential (eV)
ZnO	3.14	+2.860	−0.280
ZB4	2.97	+2.969	−0.001
ZB5	3.03	+3.001	−0.029
ZB6	3.07	+3.021	−0.049

$$\text{ARS dye} + OH^{\bullet} \rightarrow \text{Degradation products} \quad (11)$$

$$\text{ARS dye} + h^{+}\left(VB\right) \rightarrow \text{Oxidation products} \quad (12)$$

$$\text{ARS dye} + e^{-}\left(CB\right) \rightarrow \text{Reduction products} \quad (13)$$

The difference in the photocatalytic efficiency of prepared catalysts at different calcination temperatures can be explained based on the position of the conduction band (CB) and valence band (VB) calculated as in Table 1. It is seen that the maximum difference in CB potential of ZnO and ZB4, that is, the trapped electrons (e^-) remain for a longer time in CB or other words maximum charge separation takes place in ZB4 which prevents electrons-holes recombination, hence maximum photodegradation was found to be with ZB4.

4. Conclusions

α-Bi_2O_3/ZnO doped β-Bi_2O_3 photocatalyst at different calcination temperatures was synthesized by a modified sol–gel method. The results revealed that an increase in calcination temperature affects the phase and morphology of the prepared photocatalyst. The photodegradation efficiency of ZB4, ZB5, and ZB6 was evaluated using ARS dye as an organic pollutant under visible light irradiation. The maximum photocatalytic activity of ZB4 (88%) was observed as compared to ZB5 (59%) and ZB6 (51%) due to less bandgap (2.97 eV) and less phase transformation (β-Bi_2O_3 to α-Bi_2O_3) at lower temperature, that is, 400°C. Therefore, ZB4 powder calcined at lower temperature, that is, 400°C acts as an efficient photocatalyst for the degradation of organic compounds in a neutral medium under visible light illumination.

Acknowledgments

References

[1] X. Lin, P. Lv, Q. Guan, H. Li, H. Zhai, C. Liu, Bismuth titanate microspheres: directed synthesis and their visible light photocatalytic activity, Appl. Surf. Sci., 258 (2012) 7146–7153.

[2] K.P.O. Mahesh, D.-H. Kuo, B.-R. Huang, Facile synthesis of heterostructured Ag-deposited SiO_2@TiO_2 composite spheres with enhanced catalytic activity towards the photodegradation of AB1 dye, J. Mol. Catal. A: Chem., 396 (2015) 290–296.

[3] A. Senthilraja, B. Subash, P. Dhatshanamurthi, M. Swaminathan, M. Shanthi, Photocatalytic detoxification of acid red 18 by modified ZnO catalyst under sunlight irradiation, Spectrochim. Acta, Part A, 138 (2015) 31–37.

[4] W. Raza, M.M. Haque, M. Muneer, T. Harada, M. Matsumura, Synthesis, characterization and photocatalytic performance of visible light induced bismuth oxide nanoparticle, J. Alloys Compd., 648 (2015) 641–650.

[5] R. Khan, M.S. Hassan, P. Uthirakumar, J.H. Yun, M.-S. Khil, I.-H. Lee, Facile synthesis of ZnO nanoglobules and its photocatalytic activity in the degradation of methyl orange dye under UV irradiation, Mater. Lett., 152 (2015) 163–165.

[6] G. Poogodi, P. Anandan, R.M. Kumar, R. Jayavel, Studies on visible light photocatalytic and antibacterial activities of nanostructured cobalt doped ZnO thin films prepared by sol–gel spin coating method, Spectrochim. Acta, Part A, 148 (2015) 237–243.

[7] S. Raeisivand, M. Sadeghi, S. Hemati, A. Fadaei, M. Sedehi, A. Sadeghi, S.M. Hoseini, Photocatalytic degradation of catechol in aqueous solutions: a comparison between UV/Fe_2O_3 and Fe_2O_3/sunlight processes, Desal. Water Treat., 154 (2019) 340–346.

[8] F. Liu, X. Shao, S. Yang, Bi_2S_3-ZnS/graphene complexes: synthesis, characterization, and photoactivity for the decolorization of dyes under visible light, Mater. Sci. Semicond. Process., 34 (2015) 104–108.

[9] J. Ma, J. Ding, L. Yu, L. Li, Y. Kong, S. Komarneni, Synthesis of Fe_2O_3-NiO-Cr_2O_3 composites from NiFe-layered double hydroxide for degrading methylene blue under visible light, Appl. Clay Sci., 107 (2015) 85–89.

[10] Y. Huang, W. Fan, B. Long, H. Li, F. Zhao, Z. Liu, Y. Tong, H. Ji, Visible light Bi_2S_3/Bi_2O_3/$Bi_2O_2CO_3$ photocatalyst for effective degradation of organic pollutions, Appl. Catal., B, 185 (2016) 68–76.

[11] Q.I. Rahman, M. Ahmad, S.K. Misra, M.B. Lohani, Hexagonal ZnO nanorods assembled flowers for photocatalytic dye degradation: growth, structural and optical properties, Superlattices Microstruct., 64 (2013) 495–506.

[12] P. Bansal, P. Kaur, D. Sud, Heterostructured TiO_2/ZnO-excellent nanophotocatalysts for degradation of organic contaminants in aqueous solution, Desal. Water Treat., 52 (2014) 7004–7014.

[13] M. Bagheri, M. Heydari, M.R. Vaezi, Influence of reaction conditions on formation of ionic liquid-based nanostructured Bi_2O_3 as an efficient visible-light-driven photocatalyst, J. Phys. Chem. Solids, 112 (2018) 14–19.

[14] P. Chowdhury, H. Gomaa, A.K. Ray, Sacrifical hydrogen generation from aqueous triethanolamine with eosin Y-sensitized Pt/TiO_2 photocatalyst in UV, visible and solar light irradiation, Chemosphere, 121 (2015) 54–61.

[15] J. Yu, W.-F. Lin, L.-H. Leng, S.-K. Bao, J.-P. Zou, X.-B. Luo, D.-Z. Chen, S.-L. Luo, C.-T. Au, Adsorption-degradation synergetic effects on removal of methylene blue over heterostructured TiO_2/$Co_4S_{4.23}Se_{3.77}$ composites, J. Mol. Catal. A: Chem., 394 (2014) 121–128.

[16] R. Liu, P. Hu, S. Chen, Photocatalytic activity of Ag_3PO_4 nanoparticle/TiO_2 nanobelt heterostructures, Appl. Surf. Sci., 258 (2012) 9805–9809.

[17] T.N. Soitah, Y. Chunhui, Y. Yong, N. Yinghua, S. Liang, Properties of Bi_2O_3 thin films prepared via a modified pechini route, Curr. Appl. Phys., 10 (2010) 1372–1377.

[18] Y. Lu, Y. Zhao, J. Zhao, Y. Song, Z. Huang, F. Gao, N. Li, Y. Li, Photoactive β-Bi$_2$O$_3$ architectures prepared by a simple solution crystallization method, Ceram. Int., 40 (2014) 15057–15063.

[19] Z. Wang, S. Bi, Y. Wan, P. Huang, M. Zheng, Optical properties of a new Bi$_{38}$Mo$_7$O$_{78}$ semiconductor with fluorite-type δ-Bi$_2$O$_3$ structure, Appl. Surf. Sci., 399 (2017) 506–514.

[20] A. Charanpahari, S.S. Umare, R. Sasikala, Enhanced photo-degradation of dyes on Bi$_2$O$_3$ microflakes: effect of GeO$_2$ addition on photocatalytic activity, Sep. Purif. Technol., 133 (2014) 438–442.

[21] L. Zhang, P. Ghimire, J. Phuriragpitikhon, B. Jiang, A.A.S. Goncalves, M. Jaroniec, Facile formation of metallic bismuth/bismuth oxide heterojunction on porous carbon with enhanced photocatalytic activity, J. Colloid Interface Sci., 513 (2018) 82–91.

[22] Q. Wang, J. Hui, L. Yang, H. Huang, Y. Cai, S. Yin, Y. Ding, Enhanced photocatalytic performance of Bi$_2$O$_3$/H-ZSM-5 composite for rhodamine B degradation under UV light irradiation, Appl. Surf. Sci., 289 (2014) 224–229.

[23] S. Xue, H. He, Q. Fan, C. Yu, K. Yang, W. Huang, Y. Zhou, Y. Xie, La/Ce-codoped Bi$_2$O$_3$ composite photocatalysts with high photocatalytic performance in removal of high concentration dye, J. Environ. Sci., 60 (2017) 70–77.

[24] M. Ratavo, G.T. West, P.J. Kelly, X. Xia, Y. Gao, Synergistic effect of doping with nitrogen and molybdenum on the photocatalytic properties of thin titania films, Vaccum, 114 (2015) 205–212.

[25] P. Malathy, K. Vignesh, M. Rajarajan, A. Suganthi, Enhanced photocatalytic performance of transition metal doped Bi$_2$O$_3$ nanoparticle under visible light irradiation, Ceram. Int., 40 (2014) 101–107.

[26] S. Han, J. Li, K. Yang, J. Lin, Fabrication of a β-Bi$_2$O$_3$/BiOI heterojunction and its efficient photocatalysis for organic dye removal, Chin. J. Catal., 36 (2015) 2119–2126.

[27] X. Liu, H. Deng, W. Yao, Q. Jiang, J. Shen, Preparation and photocatalytic activity of Y-doped Bi$_2$O$_3$, J. Alloys Compd., 651 (2015) 135–142.

[28] V.L. Chandraboss, L. Natanapatham, B. Karthikeyan, J. Kamala-kkannan, S. Prabha, S. Senthivelan, Effect of bismuth doping on the ZnO nanocomposite material and study of its photocatalytic activity under UV-light, Mater. Res. Bull., 48 (2013) 3707–3712.

[29] C.-Y. Chen, J.-C. Weng, J.-H. Chen, S.-H. Ma, K.-H. Chen, T.-L. Horng, C.-Y. Tsay, C.-J. Chang, C.-K. Lin, J.-J. Wu, Photocatalyst ZnO-doped Bi$_2$O$_3$ powder prepared by spray pyrolysis, Powder Technol., 272 (2015) 316–321.

[30] L.-R. Hou, C.-Z. Yuan, Y. Peng, Preparation and photocatalytic property of sunlight-driven photocatalyst Bi$_{38}$ZnO$_{58}$, J. Mol. Catal. A: Chem., 252 (2006) 132–135.

[31] S. Ghattavi, A. Nezamzadeh-Ejhieh, A brief study on the boosted photocatalytic activity of AgI/WO$_3$/ZnO in the degradation of methylene blue under visible light irradiation, Desal. Water Treat., 166 (2019) 92–104.

[32] X. Zhao, S. Qu, J. Han, Photocatalytic degradation of tetracycline on g-C$_3$N$_4$/Fe$_3$O$_4$ magnetic photocatalyst, Desal. Water Treat., 150 (2019) 213–219.

[33] H. Yu, P. Xiao, J. Tian, F. Wang, J. Yu, Phenylamine-functionalized rGO/TiO$_2$ photocatalysts: spatially separated adsorption sites and tunable photocatalytic selectivity, ACS Appl. Mater. Interfaces, 8 (2016) 29470–29477.

[34] D. Li, H. Wang, H. Tang, X. Yang, Q. Liu, Remarkable enhancement in solar oxygen evolution from MoSe$_2$/Ag$_3$PO$_4$ heterojunction photocatalyst via in situ constructing interfacial contact, ACS Sustainable Chem. Eng., 7 (2019) 8466–8474.

[35] Y. Guo, Y. Ao, P. Wang, C. Wang, Mediator-free direct dual-Z-scheme Bi$_2$S$_3$/BiVO$_4$/MgIn$_2$S$_4$ composite photocatalysts with enhanced visible-light-driven performance towards carbamazepine degradation, Appl. Catal., B, 254 (2019) 479–490.

[36] M. Ren, Y. Ao, P. Wang, C. Wang, Construction of silver/graphitic-C$_3$N$_4$/bismuth tantalite Z-scheme photocatalyst with enhanced visible-light-driven performance for sulfamethoxazole degradation, Chem. Eng. J., 378 (2019) 122122–122131.

[37] Y. Fu, Z. Li, Q. Liu, X. Yang, H. Tang, Construction of carbon nitride and MoS$_2$ quantum dot 2D/0D hybrid photocatalyst: direct Z-scheme mechanism for improved photocatalytic activity, Chin. J. Catal., 38 (2017) 2160–2170.

[38] W. Liu, J. Shen, X. Yang, Q. Liu, H. Tang, Dual Z-scheme g-C$_3$N$_4$/Ag$_3$PO$_4$/Ag$_2$MoO$_4$ ternary composite photocatalyst for solar oxygen evolution from water splitting, Appl. Surf. Sci., 456 (2018) 369–378.

[39] S.A. Khayyat, M.S. Akhtar, A. Umar, ZnO nanocapsules for photocatalytic degradation of thionine, Mater. Lett., 81 (2012) 239–241.

[40] R. Kumar, G. Kumar, M.S. Akhtar, A. Umar, Sonophotocatalytic degradation of methyl orange using ZnO nano-aggregates, J. Alloys Compd., 629 (2015) 167–172.

[41] T.K. Ghorai, N. Biswas, Photodegradation of rhodamine 6G in aqueous solution via SrCrO$_4$ and TiO$_2$ nano-sphere mixed oxides, J. Mater. Res. Technol., 2 (2013) 10–17.

[42] D. Sanchez-Martinez, I. Juarez-Ramirez, L.M. Torres-Martinez, I.D. Leon-Abarte, Photocatalytic properties of Bi$_2$O$_3$ powders obtained by an ultrasound-assisted precipitation method, Ceram. Int., 42 (2016) 2013–2020.

[43] W. Shan, Y. Hu, Z. Bai, M. Zheng, C. Wei, *In situ* preparation of C$_3$N$_4$/bismuth-based oxide nanocomposites with enhanced photocatalytic activity, Appl. Catal., B, 188 (2016) 1–12.

[44] J. Lv, T. Sheng, L. Su, G. Xu, D. Wang, Z. Zheng, Y. Wu, N,S co-doped-TiO$_2$/fly ash beads composite material and visible light photocatalytic activity, Appl. Surf. Sci., 284 (2013) 229–234.

[45] N. Kannan, G.G. Nagnathan, Photocatalytic degradation of safranine dye on semiconductor by UV radiation, Int. J. Environ. Prot., 27 (2007) 1103–1108.

[46] S.K. Kansal, R. Lamba, S.K. Mehta, A. Umar, Photocatalytic degradation of alizarin red s using simply synthesized ZnO nanoparticles, Mater. Lett., 106 (2013) 385–389.

[47] A. Amalraj, A. Pius, Photocatalytic degradation of alizarin red S and bismarck brown R using TiO$_2$ photocatalyst, J. Chem. Appl. Biochem., 1 (2014) 1–7.

[48] P. Parra, V. Sarria, S. Maloto, P. Periner, C. Pulgarin, Photocatalytic degradation of attrzine using suspended and supported TiO$_2$, J. Appl. Catal., B, 51 (2004) 107–116.

[49] M.L.D. Souza, P. Corio, Effect of silver nanoparticles on TiO$_2$-mediated photodegradation of alizarin red S, Appl. Catal., A, 136–137 (2013) 325–333.

[50] N.N. Rao, S. Dube, TiO$_2$-catalysed photodegradation of reactive orange 84 and alizarin red S biological stain, Indian J. Chem. Technol., 4 (1997) 1–6.

[51] J. Hou, C. Yang, Z. Wang, S. Jiao, H. Zhu, Bi$_2$O$_3$ quantum dots decorated anatase TiO$_2$ nanocrystals with exposed {0 0 1} facets on graphene sheets for enhanced visible-light photocatalytic performance, Appl. Catal., B, 129 (2013) 333–341.

[52] N. Wetchakun, S. Chainet, S. Panichphant, K. Wetchakun, Efficient photocatalytic degradation of methylene blue over BiVO$_4$/TiO$_2$ nanocomposites, Ceram. Int., 41 (2015) 5999–6004.

[53] Y. Xu, M.A.A. Schoonen, The absolute energy positions of conduction and valence bands of selected semiconducting minerals, Am. Mineral., 85 (2000) 543–556.

[54] L. Saikia, D. Bhuyan, M. Saikia, B. Malakar, D.K. Dutta, P. Sengupta, Photocatalytic performance of ZnO nanomaterials for self sensitized degradation of malachite green dye under solar light, Appl. Catal., A, 490 (2015) 42–49.

[55] K. Yang, X. Li, C. Yu, D. Zeng, F. Chen, K. Zhang, W. Huang, H. Ji, Review on heterophase/homophase junctions for efficient photocatalysis: the case of phase transition construction, Chin. J. Catal., 40 (2019) 796–818.